Title
Dose-Response and Viral Kinetics Analysis of SARS-CoV-1 in Non-Human Primates

Author
Lee, Philip Chan

Publication Date
2023

Peer reviewed|Thesis/dissertation

UNIVERSITY OF CALIFORNIA

Los Angeles

Dose-Response and Viral Kinetics Analysis of SARS-CoV-1 in Non-Human Primates

A thesis submitted in partial satisfaction
of the requirements for the degree
Master of Science in Bioinformatics

by

Philip Chan Lee

2023

ABSTRACT OF THE THESIS

Dose-Response and Viral Kinetics
Analysis of SARS-CoV-1
in Non-Human Primates

by

Philip Chan Lee
Master of Science in Bioinformatics
University of California, Los Angeles, 2023
Professor James O. Lloyd-Smith, Chair

Dose-response models are a key component of quantitative microbial risk assessment and can be used to estimate the infectious and lethal doses of novel emerging pathogens to help inform control and prevention measures. Unfortunately, obtaining estimates of infectious and lethal doses in humans can be difficult due to ethical constraints and limited data from experimental challenge studies of relevant animal models such as non-human primates (NHPs). NHP challenge studies tend to have small sample sizes and there are often only one or two dose levels within a single study, which makes dose-response modeling infeasible using data from single studies. Here, by using Bayesian computational methods, we developed an approach to aggregate NHP pathogen load data across multiple challenge studies in order to simultaneously analyze the dose-response relationship and within-host kinetics. We tested our approach by aggregating NHP viral load data across six SARS-CoV-1 challenge studies, and we obtained the first-ever ID_{50} estimates for SARS-CoV-1 in NHPs. Our work demonstrated the value in reusing previous data from animal experiments, and the modeling

framework we developed can be applied to other pathogens, especially in cases where data is limited within individual studies.

The thesis of Philip Chan Lee is approved.

Nandita Garud

Kirk E. Lohmueller

James O. Lloyd-Smith, Committee Chair

University of California, Los Angeles

2023

TABLE OF CONTENTS

LIST OF FIGURES

LIST OF TABLES

ACKNOWLEDGMENTS

I would like to thank Dr. Jamie Lloyd-Smith for his mentorship and all of the members of the Lloyd-Smith lab for their advice and encouragement. I would like to thank Celine Snedden and Dr. Dylan Morris for helping me with developing my dose-response model and for teaching me Bayesian inference.

I would also like to thank my committee members, Dr. Nandita Garud and Dr. Kirk Lohmueller, for taking the time to help me with my thesis and for teaching me about statistics in ecological research.

Finally, I would like to thank my parents for their support and for inspiring me to pursue a career in science.

1. Introduction

The past two decades have seen the emergence of several novel infectious pathogens. Many of these emerging pathogens have zoonotic origins, and they have been responsible for significant financial costs and loss of human life. Additionally, given recent changes in human demographics and behavior, such as increasing urbanization, population sizes, and air travel, as well as changes in patterns of land use, we should expect to continue seeing new emerging diseases in the future. One of the major obstacles in controlling these novel emerging diseases is data scarcity, especially during the early stages of an outbreak. Although there currently exist many well-established modeling frameworks for studying between-host and within-host spread of pathogens, without sufficient data it can be difficult to forecast disease burden and determine proper intervention measures. Thus, there is a need for new methods that can make the most of limited data across disparate sources in order to perform modeling analyses.

Here we focus on dose-response models, which are a key component of the quantitative microbial risk assessment (QMRA) framework. Dose-response models are used to quantify the risk of a given response (e.g., infection or death) to given doses of pathogen [8]. These models can be used to generate estimates of the infectious and lethal doses of pathogens, which are the doses that are required in order to reliably cause infection or mortality in an individual (e.g., the ID_{50} is the dose that produces infection in 50% of hosts). Obtaining estimates of the infectious dose, such as the ID_{50}, is especially useful for informing control policies early in an outbreak. For example, a pathogen with a very low infectious dose might

indicate high transmissibility between individuals and thus support the need for control measures that reduce even brief exposures.

Unfortunately, obtaining reliable estimates for infectious and lethal doses in humans is typically challenging due to limitations of the available data and the types of experiments that can be performed. In cases where the pathogen of interest causes significant risk of severe disease or death in humans (which makes controlled human infections unethical), dose-response model estimates must primarily rely on data from animal experiments, often using rodents or ferrets [10]. Although these small animal model experiments are more feasible, and it is possible to obtain larger sample sizes which bolster statistical analyses, there are clearly inherent limitations when trying to extrapolate results from these data to human infections [3]. For example, early in the COVID-19 pandemic the best guess at the infectious dose for SARS-CoV-2 in humans came from a study of SARS-CoV-1 in transgenic mice, and the knowledge gap on human infectious dose was cited repeatedly as a limitation in guiding control policy [25].

A natural route to obtain more human-relevant infectious dose estimates would be to apply dose-response modeling approaches to data from animal models that are more closely related to humans, such as non-human primates (NHPs). However, working with data from NHP experiments is also challenging. Due to important ethical and logistical considerations, NHP experiments tend to have small sample sizes, which makes it difficult to perform quantitative analyses using data obtained from a single experiment. Furthermore, NHP studies often have goals other than dose-response modeling, such as studying disease pathogenesis or countermeasures, so animals are usually inoculated with just one or two dose levels within a single study. To perform dose-response modeling with NHPs in the absence of dose-response experiments, data needs to be aggregated across multiple studies in a principled way.

A further complication involved in working with NHP experiment data – and particularly in seeking to aggregate data across studies – comes from the variety and richness of the data collected. After inoculation with a pathogen of interest, animals are often sampled at multiple

time points in multiple different body locations (e.g., nasal/oral swabs, rectal swabs, blood samples) and with multiple assays (e.g., immunological measurements, PCR results, culture results). This can make it difficult to define what it means for an individual to be "infected" or "non-infected." However, there is also a great opportunity to leverage these data to learn more about dose effects beyond just simple infectivity. Traditional dose-response models require individuals to be classified via a binary infectivity scheme, either infected or non-infected. However, there is clearly individual-level variation in responses to infection, and there are many cases where it would be useful to define a continuum of disease responses. In particular, for experiments that report quantitative measurements (e.g., C_T or viral load values for quantitative PCR results), there is the opportunity to investigate potential dose effects on within-host viral kinetics.

Here, we developed an approach to aggregate and reuse data from experimental challenge studies of NHPs to perform dose-response modeling, both to obtain estimates of the infectious dose and to evaluate potential dose effects on within-host viral kinetics. To demonstrate our approach, we collected virological data across six SARS-CoV-1 NHP challenge studies, resulting in a dataset of 39 individuals. Our dataset represented four inoculation doses (ranging from 10^3 $TCID_{50}$ to $10^{6.9}$ $TCID_{50}$). We developed a joint dose-response and viral kinetics framework, which included a mechanistic model to link dose-infectivity to the dynamics of viral RNA in the upper respiratory tract (URT) of NHPs. Our framework also utilized Bayesian computational methods to flexibly integrate data and account for possible between-study biases. By fitting our model to observed URT viral load measurements in our dataset, we were able to simultaneously: (i) estimate the probability that each individual NHP was infected, (ii) evaluate the effect of inoculation dose on the magnitude and timing of the viral load trajectories, and (iii) generate the first-ever ID_{50} estimates of SARS-CoV-1 in NHPs. The work here represents the first-ever dose-response analysis of SARS-CoV-1 in NHPs, and it demonstrates the value in reusing virological data from previous animal challenge experiments. Additionally, the framework presented here can be applied to other

pathogens to investigate dose effects beyond infectivity, especially in cases where data is limited within studies or where it is difficult to classify individuals as infected or non-infected.

2. Methods

2.1 Data Collection

We performed a comprehensive literature search for SARS-CoV-1 NHP challenge studies. To be included in our analysis, an article was required to: (i) be a primary study involving experimental infection of rhesus macaques (*Macaca mulatta*) or cynomolgus macaques (*Macaca fascicularis*) with a strain of SARS-CoV-1 that had not been genetically modified, and (ii) report quantitative virological data. We found that the most common inoculation procedure involved intranasal inoculation using nasal drops. For consistency, we only included studies in our analysis that performed intranasal inoculation of NHPs and reported viral load data from URT swabs (since intranasal inoculation with drops primarily leads to URT infections) [28]. In total, six studies were included in our dose-response and viral kinetics analysis (Table 2.1). Raw data was not published in any of the six studies, so viral load values were manually extracted from the texts, tables, and figures. Data from figures were extracted using the R package digitize (version 0.0.4) [20].

Our final dataset contained viral load data from 37 individuals inoculated with SARS-CoV-1 intranasally and two individuals inoculated with SARS-CoV-1 via a combined intranasal and conjunctival route (50/50 split of the inoculum between the nose and conjunctiva). These last two individuals were included in our analysis because fluid deposited in the eye largely drains to the nasal cavity via the nasolacrimal duct [2], and thus these individuals should experience responses similar to individuals inoculated solely through the nose.

Table 2.1: *Summary of studies included in the dose-response and kinetics analysis.* The number in parentheses in the "Number of Individuals" column is the cumulative number of viral load measurements taken from individuals in that study.

Study	Strain	Dose(s)	Macaque Species	Swab Type(s)	Number of Individuals
Li et al., 2005 [13]	PUMC01	10^5 $TCID_{50}$	Rhesus	Oral	8 (8)
Lawler et al., 2006* [12]	Urbani	6×10^6 PFU	Cynomolgus	Nasal, Oral	2 (46)
Nagata et al., 2007 [19]	HKU-39849	10^3, 10^6 $TCID_{50}$	Cynomolgus	Nasal, Oral	4 (38)
Chen et al., 2008 [5]	PUMC01	10^5 $TCID_{50}$	Rhesus	Oral	11 (11)
Liu et al., 2016 [14]	PUMC01	10^5 $TCID_{50}$	Rhesus	Oral	12 (72)
Liu et al., 2019 [15]	PUMC01	10^5 $TCID_{50}$	Rhesus	Oral	2 (5)

*Individuals inoculated via a combined intranasal and conjunctival route

The 39 individuals in our dataset represented four unique inoculation doses (10^3 $TCID_{50}$, 10^5 $TCID_{50}$, 10^6 $TCID_{50}$, 6×10^6 PFU) and 180 viral load measurements from URT swabs (nasal and oral swabs). Lawler et al. was the only study that reported inoculation doses in units of PFU, so a conversion factor of 0.7 was used to convert the PFU dose to units of $TCID_{50}$: 6×10^6 PFU / $0.7 \approx 10^{6.9}$ $TCID_{50}$ [4].

2.2 Joint Dose-Response and Kinetics Model

We developed a framework to simultaneously perform a dose-response analysis as well as a within-host kinetics analysis of SARS-CoV-1 in NHPs (Figure 2.1).

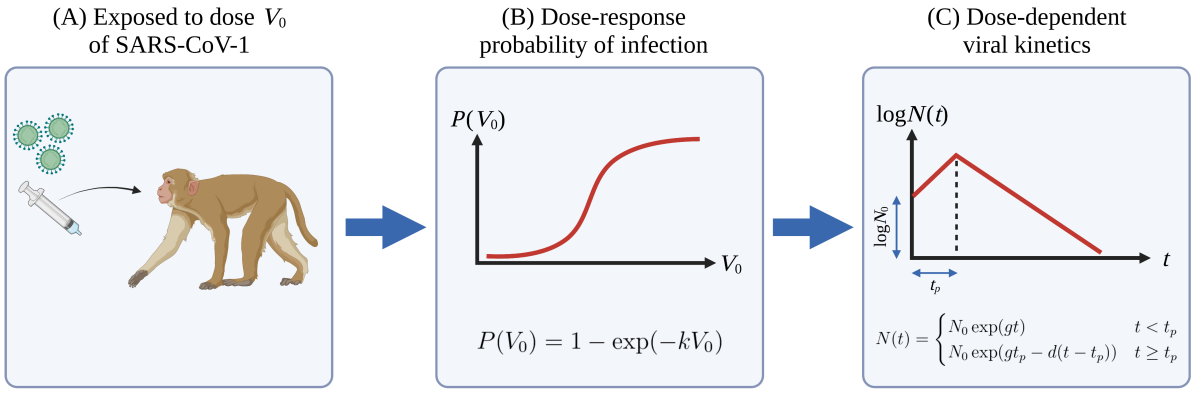

Figure 2.1: *Dose-response and viral kinetics model for SARS-CoV-1 inoculations in non-human primates.* An individual NHP is exposed to a dose V_0 of SARS-CoV-1 (A), which results in a probability of infection given by the exponential dose-response curve (B). Given a successful infection, viral RNA can be observed in URT swabs as measured viral load values, which follow a pattern of exponential growth and decay (C).

2.2.1 Dose-Response Model

We used a single-hit, independent action, exponential dose-response model for the SARS-CoV-1 infection process in NHPs following intranasal inoculation. In this model, if the host is exposed to V_0 virions, then the number of successful virions, V_s, is Poisson distributed with mean kV_0, where k is the hit probability (i.e., the per virion success probability) [8]. The probability that the host is infected ($V_s > 0$) after exposure to V_0 virions is

$$P(V_0) = 1 - \exp(-kV_0)$$

2.2.2 Viral Kinetics Model

Following a successful infection, we modeled the within-host virus dynamics as exponential growth up to a peak time and then exponential decay afterwards. Our model for the measured viral load from URT swabs, $N(t)$, was

$$N(t) = \begin{cases} N_0 \exp(gt) & t < t_p \\ N_0 \exp(gt_p - d(t - t_p)) & t \geq t_p \end{cases}$$

where N_0 is the initial viral load established immediately following the inoculation, t_p is the time of peak viral load, g is the growth rate, and d is the decay rate.

2.2.3 Dose-Dependence of Kinetics

We included in our model the possibility that the initial viral load and time of peak viral load vary in a dose-dependent manner. First, given that infection was successful ($V_s > 0$), the expected number of successful virions is

$$\bar{V}_s = \frac{kV_0}{1 - \exp(-kV_0)}$$

which is the mean of the zero-truncated Poisson distribution of V_s. Next, we encoded the dependence of the initial viral load and time of peak viral load with log-log linear relationships:

$$\log(N_0) = \alpha_N[\log(\bar{V}_s) - \log(\bar{V}_{s,10^5})] + \beta_N$$
$$\log(t_p) = \alpha_t[\log(\bar{V}_s) - \log(\bar{V}_{s,10^5})] + \beta_t$$

To improve the interpretability of the β_N and β_t parameters, we included a horizontal shift of $\log(\bar{V}_{s,10^5})$, where $\bar{V}_{s,10^5}$ is the expected number of successful virions given an inoculation dose of 10^5 TCID_{50}. By encoding the dependence in this way, we allowed for several possible relationships between the viral kinetics parameters and the initial inoculation dose. The magnitude and sign of the slope parameters, α_N and α_t, control the strength and direction of the dose-dependence of initial viral load and time of peak viral load. The intercept parameters, β_N and β_t, represent the log initial viral load and log time of peak viral load

given an inoculation dose of 10^5 $TCID_{50}$.

2.3 Fitting the Model to NHP Viral Load Data

We used Bayesian inference to fit our joint dose-response and kinetics model to our dataset of non-human primate URT swab PCR measurements. Our dataset contained 180 total measurements, and these measurements included both numeric viral load values (which are always greater than 0) as well as binary values (i.e., detected or not detected, "+" or "−"). Suppose an individual NHP had viral load measurements n_t at various times t. There are two cases to consider for the data likelihood: (i) the viral load measurements were observed given the individual was infected and (ii) the viral load measurements were observed given the individual was non-infected.

2.3.1 Modeling Successful Infections

Given that the individual was successfully infected, we modeled numeric values of n_t around our predicted values (i.e., values from the viral kinetics model) with a log-normal distribution:

$$\log(n_t) \sim \text{Normal}(\log(N(t)), \sigma_s)$$

where σ_s accounts for measurement variation.

For binary values, we integrated over the possible ranges of viral load values using the same log-normal distribution for the numeric values. For an undetected measurement (−), we integrated over the viral load range $(-\infty, \log(L)]$, and for a detected measurement (+), we integrated over the viral load range $[\log(L), \infty)$, where L is the lower limit of detection of the PCR assay.

Lawler et al. was the only study included in our analysis that reported a lower limit of detection for their PCR assay. For the each of the remaining studies, we used the smallest

reported viral load value from the study as the effective limit of detection.

2.3.2 Modeling Unsuccessful Infections

Given that the individual was not successfully infected, the probability of observing a numeric or detected (+) value is p_{falsepos}, which is the false positive probability. This parameter captures the possible (but unlikely) technical errors (e.g., sample contamination) that might occur during the course of the experiments. If the measured value was undetected (−), then the probability of observing the measurement (a true negative) is $1 - p_{\text{falsepos}}$.

2.4 Prior Distributions

Overall, we sought to set "weakly informative" prior distributions for our model parameters. The goal was to rule out biologically implausible parameters values while at the same time allowing a wide range of biologically plausible parameter values.

2.4.1 Infectious Dose and Hit Probability

For improved interpretability, we placed a prior on the ID_{50} rather than the hit probability, where $k = \log(2)/\text{ID}_{50}$. We placed a log-normal prior on the ID_{50}, with the ID_{50} in units of TCID_{50}:

$$\log(\text{ID}_{50}) \sim \text{Normal}(\log(10^4), \log(10))$$

2.4.2 Viral Kinetics Parameters

For improved interpretability, we placed priors on the doubling and halving times (units of days) of the viral load kinetics rather than the growth and decay rates. The doubling time is $t_2 = \log(2)/g$, and the halving time is $t_{\frac{1}{2}} = \log(2)/d$.

To account for the fact that not all studies used the same strains of SARS-CoV-1 and macaque species, we added study-level hierarchy to these parameters, where t_{2i} and $t_{\frac{1}{2}i}$ are the doubling and halving times for study i. The log doubling times are distributed around μ_{t2} with standard deviation σ_{t2}, and the log halving times are distributed around $\mu_{t_{\frac{1}{2}}}$ with standard deviation $\sigma_{t_{\frac{1}{2}}}$:

$$\begin{aligned}
\log(t_{2i}) &\sim \text{Normal}(\mu_{t2}, \sigma_{t2}) \\
\mu_{t2} &\sim \text{Normal}(\log(0.5), 0.5) \\
\sigma_{t2} &\sim \text{PosNormal}(0, 0.35) \\
\log(t_{\frac{1}{2}i}) &\sim \text{Normal}(\mu_{t_{\frac{1}{2}}}, \sigma_{t_{\frac{1}{2}}}) \\
\mu_{t_{\frac{1}{2}}} &\sim \text{Normal}(\log(2), 0.75) \\
\sigma_{t_{\frac{1}{2}}} &\sim \text{PosNormal}(0, 0.35)
\end{aligned}$$

2.4.3 Dose-Dependence Parameters

For the initial viral load slope parameter, α_N, we placed a prior on the difference between the log initial viral load for 10^7 and 10^5 TCID_{50} inoculated individuals, $\log(N_{0,10^7}) - \log(N_{0,10^5})$. Similarly, for the time of peak viral load slope parameter, α_t, we placed a prior on the difference between the log peak time for 10^7 and 10^5 TCID_{50} inoculated individuals, $\log(t_{p,10^7}) - \log(t_{p,10^5})$. The priors were:

$$\begin{aligned}
\log(N_{0,10^7}) - \log(N_{0,10^5}) &\sim \text{Normal}(\log(100), 1.5) \\
\log(t_{p,10^7}) - \log(t_{p,10^5}) &\sim \text{Normal}(0, 1)
\end{aligned}$$

The slope parameters can then be calculated as

$$\alpha_N = \frac{\log(N_{0,10^7}) - \log(N_{0,10^5})}{\log(\bar{V}_{s,10^7}) - \log(\bar{V}_{s,10^5})}$$
$$\alpha_t = \frac{\log(t_{p,10^7}) - \log(t_{p,10^5})}{\log(\bar{V}_{s,10^7}) - \log(\bar{V}_{s,10^5})}$$

where $\bar{V}_{s,10^7}$ and $\bar{V}_{s,10^5}$ correspond to the expected number of successful virions given an inoculation dose of 10^7 and 10^5 TCID_{50}, respectively.

We placed normal priors on the intercept parameters, β_N and β_t. To account for between-study variation (e.g., one study tends to measure higher viral loads than other studies), we added study-level hierarchy to these parameters, where β_{Ni} and β_{ti} are the intercept parameters for study i. The log initial viral load intercept parameters are distributed around $\mu_{\beta N}$ with standard deviation $\sigma_{\beta N}$, and the log time of peak viral load intercept parameters are distributed around $\mu_{\beta t}$ with standard deviation $\sigma_{\beta t}$:

$$\begin{aligned}
\beta_{Ni} &\sim \text{Normal}(\mu_{\beta N}, \sigma_{\beta N}) \\
\mu_{\beta N} &\sim \text{Normal}(\log(10^3), \log(10)) \\
\sigma_{\beta N} &\sim \text{PosNormal}(0, 0.35) \\
\beta_{ti} &\sim \text{Normal}(\mu_{\beta t}, \sigma_{\beta t}) \\
\mu_{\beta t} &\sim \text{Normal}(\log(2), 0.5) \\
\sigma_{\beta t} &\sim \text{PosNormal}(0, 0.35)
\end{aligned}$$

2.4.4 Measurement Variation

We placed priors on the measurement variation parameters, σ_s. To account for between-study variation, we added study-level hierarchy to these parameters, where σ_{si} is the measurement

variation for study i:

$$\sigma_{si} \sim \text{PosNormal}(0, 1)$$

2.4.5 False Positive Probability

We placed a log-normal prior on the false positive probability:

$$\log(p_{\text{falsepos}}) \sim \text{Normal}(\log(10^{-4}), \log(1.5))$$

2.5 Computational Methods

We used Markov Chain Monte Carlo methods to estimate all of the model parameters. We implemented and conducted inference in R using the Stan platform. Posterior samples were drawn using Stan via the R interface RStan [24]. We used four Markov chains, each with 4000 iterations (including warmup). Convergence was assessed by checking the potential scale reduction factor (PSRF) for each parameter.

Data preparation, analysis, and visualizations were completed in R using the packages dplyr, ggplot2, and tidybayes [11, 26, 27].

3. Results

3.1 Estimates of Infectious Dose for SARS-CoV-1 in Non-Human Primates

We fitted our joint dose-response and kinetics model to URT viral load data collected from 39 rhesus and cynomolgus macaques that were intranasally or intranasally and conjunctivally inoculated with SARS-CoV-1.

The posterior median ID_{50} was $10^{3.57}$ $TCID_{50}$ (95% credible interval: $[10^{1.97}, 10^{4.28}]$) (Figure 3.1A). The NHP SARS-CoV-1 challenge studies in our analysis represented four different inoculation doses: 10^3 $TCID_{50}$, 10^5 $TCID_{50}$, 10^6 $TCID_{50}$, and 6×10^6 PFU (approximately $10^{6.9}$ $TCID_{50}$). Using the exponential dose-response curve corresponding to independent action of the viral particles, these four doses had posterior median probabilities of infection of 0.168 (95% CI: $[0.036, 0.999]$), 1.000 (95% CI: $[0.974, 1.000]$), 1.000 (95% CI: $[1.000, 1.000]$), and 1.000 (95% CI: $[1.000, 1.000]$), respectively. For individuals inoculated with doses greater than 10^5 $TCID_{50}$ our model predicted that successful infection was essentially guaranteed, but for lower doses there was greater uncertainty in the estimate for infection probability, with a much wider distribution of estimated values (Figure 3.1B).

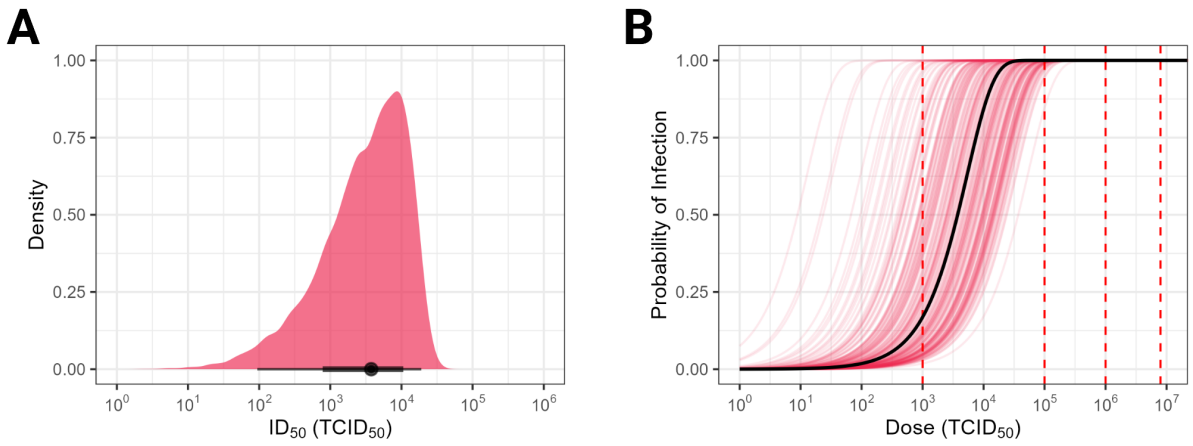

Figure 3.1: *Estimated infectious doses and infection probabilities.* (A) Inferred posterior distribution of infectious dose 50 (ID_{50}) values for SARS-CoV-1 infections in non-human primates following intranasal inoculations. The black point represents the median ID_{50} value, and the thick and thin black bars indicate the 66% and 95% credible intervals, respectively. (B) Exponential dose-response curves for 200 sampled hit probabilities from the inferred posterior distribution. The black curve shows the median estimated dose-response curve. The dotted red vertical lines indicate doses used in the included studies.

3.2 Simulations of Viral Load Kinetics for SARS-CoV-1 in Non-Human Primates

The viral kinetics component of our model allowed us to predict viral load trajectories in URT swabs for each of the studies included in our analysis (Figure 3.2A). The posterior predicted viral load trajectories further highlighted the fact that our model predicted individuals inoculated with a dose of at least 10^5 $TCID_{50}$ had a very high chance of successful infection and viral replication in the URT, while lower dose individuals had a greater chance of escaping infection (many predicted failed infections for individuals that receive 10^3 $TCID_{50}$ dose). Additionally, individuals that received larger inoculation doses were predicted to have higher initial viral loads (Figure 3.2B), higher peak viral loads (Figure 3.2C), and greater cumulative viral load (as measured by area under the viral load curve; Figure 3.2E). The relationship between inoculation dose and duration of infection (i.e., total time spent with

a viral load of at least 1) was less clear (Figure 3.2D). Overall, it appeared that larger inoculation doses resulted in longer durations of infection, but the distributions for the lower doses had very long tails due to the sparsity of data to estimate decay rates.

For the high-dose individuals (inoculation dose of at least 10^5 $TCID_{50}$), the predicted viral load trajectories aligned reasonably well with the observed trajectories. In particular, the $10^{6.9}$ $TCID_{50}$ dose individuals had many reported measurements at later time points, so there was less uncertainty in the posterior estimates for the viral load decay rate in this study. The predicted trajectories for the $10^{6.9}$ $TCID_{50}$ dose individuals clustered together closely even at later times, which helped to explain the narrower distribution of infection durations for this dosage (Figure 3.2D) and demonstrated the value of measuring extended time series data.

The predicted 10^3 $TCID_{50}$ trajectories (given that infection was successful) were clustered less tightly than the predicted trajectories for high-dose individuals. This was expected as none of the 10^3 $TCID_{50}$ dose individuals had any detectable viral RNA, and thus the predicted successful trajectories for this dosage had to be extrapolated from the higher dose individual data. Furthermore, many of the predicted successful viral load trajectories for the 10^3 $TCID_{50}$ dose individuals were below the effective limit of detection, so it was possible that the 10^3 $TCID_{50}$ dose individuals were successfully infected but had viral loads too low to be detected by the qPCR assays. This fact combined with the small number ($n = 2$) of 10^3 $TCID_{50}$ dose individuals accounted for the greater uncertainty in infection probability for low-dose individuals (Figure 3.1B).

3.3 Dose-Dependence of SARS-CoV-1 Viral Load Kinetics in Non-Human Primates

Our viral load kinetics model allowed us to assess the effect of inoculation dose on the resulting viral load trajectories. In particular, we allowed the magnitude of initial viral load

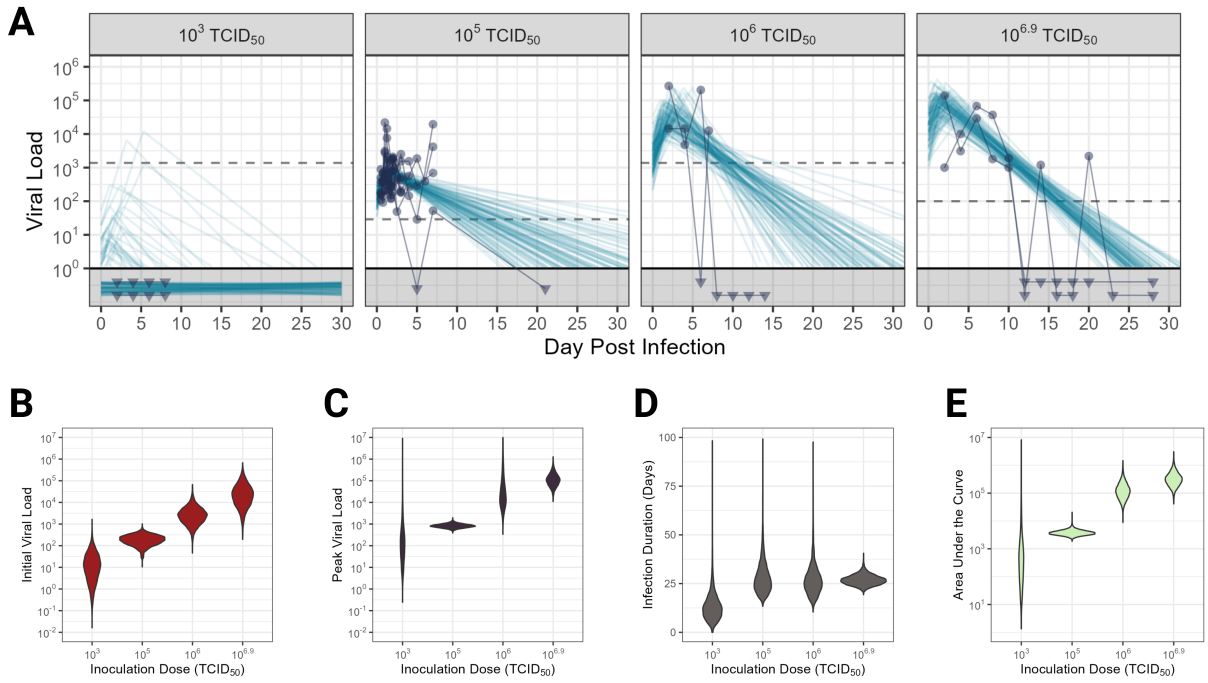

Figure 3.2: *Results for predicted URT swab viral load trajectories.* (A) Each panel shows the observed viral load trajectories in URT swabs for individuals inoculated with a given dose of SARS-CoV-1: 10^3 TCID$_{50}$ (Nagata et al., 2007), 10^5 TCID$_{50}$ (Liu et al., 2016 and Liu et al., 2019), 10^6 TCID$_{50}$ (Nagata et al., 2007), and $10^{6.9}$ TCID$_{50}$ (Lawler et al., 2006). Each point represents a measured viral load value from an oral swab, and lines connecting multiple points represent measurements taken from the same individual over time. Upside down triangles plotted in the gray region below 100 indicate measurements below the limit of detection (LOD). Horizontal dotted lines indicate the LOD ($10^{6.9}$ TCID$_{50}$ dose plot) or effective LOD (10^3, 10^5, 10^6 TCID$_{50}$ dose plots) (i.e., smallest measured value from that study). Semitransparent blue lines are 100 random draws from the inferred within-host viral load kinetics (i.e., predicted viral load trajectories based on parameter sets drawn from the joint posterior distributions), and lines that fall in the gray region indicate predicted failed infections. (Note: observed data for nasal swabs were excluded for clarity. Data from Li et al. and Chen et al. were also excluded for clarity). (B), (C), (D), (E) summarize the distributions of various metrics of the simulated trajectories at each of the four doses.

(viral load value immediately after inoculation, effectively at 0 dpi) and timing of peak viral load (dpi when viral load transitions from exponential growth to exponential decay) to vary in a dose-dependent manner.

Our model predicted a clear positive relationship between the initial viral load and inoculation dose (Figure 3.3A), i.e., larger inoculation doses lead to larger initial viral loads, which is also visible in the simulated trajectories (Figure 3.2B). The median slope parameter for the initial viral load (α_N) was 1.07 (95% credible interval: $[0.57, 1.53]$). The fact that the median value for α_N was roughly one indicated that a linear relationship between the inoculation dose and initial viral load is a highly plausible explanation for the patterns in our dataset, which is consistent with the independent action hypothesis for microbial infections (i.e., no synergistic effects between individual SARS-CoV-1 virions). For example, the median fold change in initial viral load after a 10^2-fold increase in inoculation dose (from 10^5 TCID_{50} to 10^7 TCID_{50}) was $10^{2.15}$ (95% credible interval: $[10^{1.14}, 10^{3.06}]$) (Figure 3.3C).

Conversely, our model did not predict a clear relationship between the timing of peak viral load and inoculation dose (Figure 3.3B). The median slope parameter for the timing of peak viral load (α_t) was 0.03 (95% credible interval: $[-0.27, 0.27]$). The median fold change in peak timing after a 10^2-fold increase in inoculation dose (from 10^5 TCID_{50} to 10^7 TCID_{50}) was $10^{0.07}$ (95% credible interval: $[10^{-0.55}, 10^{0.55}]$) (Figure 3.3C). A highly plausible explanation for the patterns of viral load kinetics in our dataset is that the inoculation dose did not impact the timing of peak viral load. However, the alternatives where peak timing is either positively or negatively associated with inoculation dose cannot be ruled out.

3.4 Sensitivity to Variations in Study Design

Across the six studies included in our analysis, there were two different NHP species (rhesus macaques, cynomolgus macaques), two different swab types (nasal, oral), and three different SARS-CoV-1 strains (Urbani, HKU-39849, PUMC01). To evaluate whether there were any

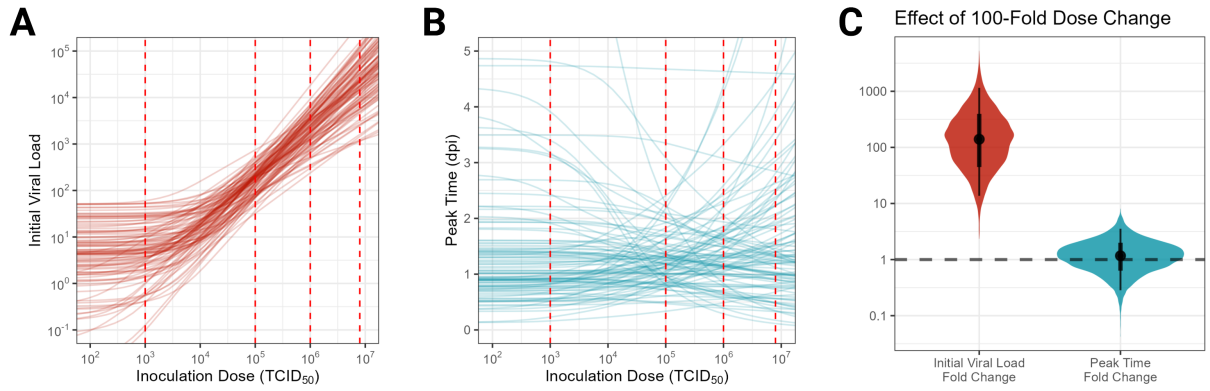

Figure 3.3: *Results for dose-dependence of viral kinetics parameters.* Relationship between the initial viral load (A) and time of peak viral load (B) with the inoculation dose. Semitransparent lines are 100 random draws from the inferred posterior relationship. The non-linearity of these inferred curves comes from the fact that we encoded the log initial viral load and log peak time as functions of the mean of the zero-truncated Poisson distribution of the number of successful virions (i.e., these plots were generated assuming that infection was successful). Dotted red vertical lines indicate doses that were used in the selected non-human primate challenge studies. (C) Inferred distributions of the effect of a 100-fold dose change (10^5 to 10^7 TCID_{50}) on the initial viral load and time of peak viral load. The dotted black horizontal line indicates no effect of inoculation dose on the viral kinetics parameters.

issues with combining data across these studies, we repeated our model fitting procedure with various subsets of the combined dataset.

Most of the URT measurements in our dataset were oral swabs (138/180 measurements). We fitted our model to only oral swab data, which resulted in parameter estimates that were very similar to the estimates obtained when we used the full dataset (results not reported here). We also fitted our model to only nasal swab data, which resulted in similar parameter results for the viral load kinetics (results not reported here). However, since the nasal swab data did not include any 10^5 $TCID_{50}$ dose individuals, the model predicted a higher median ID_{50} of $10^{4.16}$ $TCID_{50}$ (95% CI: $[10^{2.49}, 10^{5.53}]$) (Figure 3.4A). This was expected as 33/33 of the 10^5 $TCID_{50}$ dose individuals had detectable viral RNA in their oral swabs and were thus very likely successfully infected, providing strong information that the ID_{50} is well below 10^5 $TCID_{50}$; without this data, the model had trouble rejecting larger ID_{50} values. Since the model estimates did not differ in unexpected ways when fit to only oral swab data or nasal swab data, it was reasonable to combine data across these two swab types for our analysis.

To investigate whether the results were different between NHP species, we fitted our model to only data from cynomolgus macaques, which included data from Lawler et al. and Nagata et al. Similar to when we fit our model to only nasal swab data, since Lawler et al. and Nagata et al. did not have any 10^5 $TCID_{50}$ individuals, the model predicted a higher median ID_{50} of $10^{4.16}$ $TCID_{50}$ (95% CI: $[10^{2.71}, 10^{5.51}]$). We also fitted our model to data from just Nagata et al. since this was the only study where NHPs were inoculated intranasally with more than one inoculation dose. The median ID_{50} in this case was $10^{4.14}$ $TCID_{50}$ (95% CI: $[10^{2.31}, 10^{5.61}]$). Again, the model estimates did not differ unexpectedly when we fit our data to these subsets (Figure 3.4B).

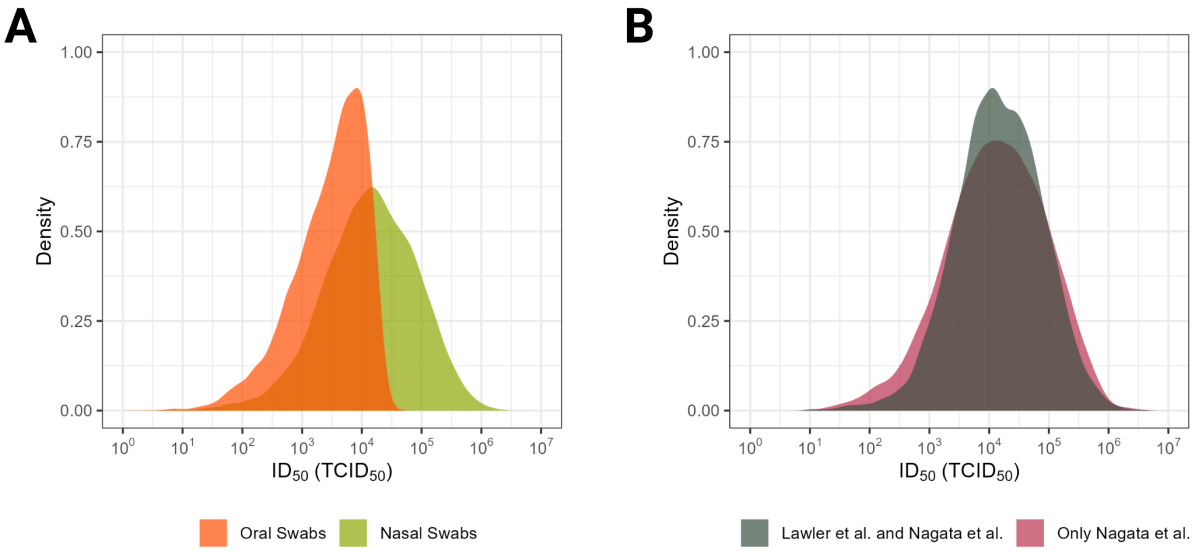

Figure 3.4: *Results for sensitivity analysis.* (A) Inferred posterior distributions of ID_{50} values using data for different swab types in our dataset. (B) Inferred posterior distributions of ID_{50} values using data from only cynomolgus macaques (data from Lawler et al. and Nagata et al.). Since Nagata et al. included two dose levels, it was also possible to estimate the ID_{50} from this study individually.

4. Discussion

In this study, we developed a joint dose-response and viral kinetics modeling framework to analyze data from SARS-CoV-1 NHP challenge studies. Our model included study-level hierarchy for several key parameters, which allowed us to aggregate NHP viral load data across multiple studies in order to obtain a sufficient number of individuals and range of inoculation doses to perform a dose-response analysis. From the dose-response component of our model, we obtained a median ID_{50} estimate of $10^{3.57}$ $TCID_{50}$ for SARS-CoV-1 via intranasal inoculations in rhesus and cynomolgus macaques. Additionally, the viral kinetics component of our model allowed us to assess the impact of inoculation dose on viral load kinetics in the URT following a successful infection. Our model predicted that larger inoculation doses resulted in higher initial viral loads, which means that infections resulting from larger exposure doses tend to start with larger concentrations of detectable viral RNA. However, there was no evidence that the timing of peak viral load (i.e., the time when the concentration of viral RNA is at a maximum) was impacted by the size of the inoculation dose.

Our estimate of the ID_{50} is the first-ever estimate for the infectious dose of SARS-CoV-1 in NHPs. Previously, a dose-response model for SARS-CoV-1 was developed by Watanabe et al., where they estimated the infectious dose of SARS-CoV-1 in transgenic mice [25]. In their model, Watanabe et al. used an exponential dose-response curve fitted to a combined dataset, from transgenic mice (expressing human ACE2) challenged with SARS-CoV-1 and unaltered mice challenged with the mouse virus MHV-1. They estimated an ID_{50} of 280

PFU, which was much lower than our estimate. The transgenic mice used in Watanabe et al. have been shown to be highly susceptible to SARS-CoV-1, with infectious virus even being detected in the brains of the mice following inoculation [6, 18]. It was thus likely that the datasets used in Watanabe et al. overestimated the infectiousness of SARS-CoV-1 in humans. In another study, Roberts et al. performed 15 serial passages of SARS-CoV-1 through BALB/c mice and obtained a virus that had an LD_{50} of $10^{4.6}$ $TCID_{50}$ in mice, which was higher than our estimate [22]. Even after the 15 passages through mice, it was possible that the adapted virus still underestimated the virulence of SARS-CoV-1 in humans since wild type SARS-CoV-1 does not result in death in unaltered mice. Our median ID_{50} estimate falls between these previous estimates of infectious dose and lethal dose in mice, and, given the greater relatedness and physiological similarities between NHPs and humans, is likely a better estimate of the human SARS-CoV-1 infectious dose.

One of the main challenges of this analysis was developing a principled way to aggregate and utilize data across the different studies. The most common data type collected and reported in the NHP SARS-CoV-1 challenge studies was viral load data, as determined by quantitative PCR, so we used these data in our analysis. However, incorporating additional data types (e.g., serology, infectious virus titers) could help to tighten the bounds on our parameter estimates even more. For example, there were very few low-dose individuals in our dataset, so our model had difficulty refining the lower bound for the ID_{50} estimates. The low-dose individuals were all from Nagata et al., and they reported that these individuals did not seroconvert, had no detectable infectious virus or viral RNA (nasal, oral, rectal swabs) up to 8 dpi, and had no detectable antibodies (by indirect fluorescence and neutralizing antibody tests) up to 8 dpi, and they concluded that infection failed to establish in these individuals [19]. This type of information can be easily incorporated into our model (i.e., the likelihood computation) and could help with tightening the ID_{50} estimates by increasing the probability that the low-dose individuals were non-infected. Unfortunately, since these additional measurements were not always reported in the other studies, it was not feasible

to incorporate this information systematically into our model.

Another limitation of the NHP data was that many of the individuals lacked extensive time series data. Out of the 39 individuals in our combined dataset, 20 individuals had only a single viral load measurement. Additionally, only 10 of the individuals had viral load measurements taken on or after 7 dpi. The lack of extensive time series data, especially measurements for later times, made it more challenging to estimate decay rates and the overall viral load trajectories. With a richer dataset with more time series data, a natural extension to our current model would be to incorporate individual-level hierarchy. The two individuals from Lawler et al. had the most time points (11 measurements taken from 2 to 28 dpi), and these data in particular highlight the fact that there are individual heterogeneities in viral load kinetics (one of the individuals peaked earlier, and one of the individuals peaked later). More extensive time series data could reveal such individual heterogeneities, which represent differential responses to infection and are key to understanding phenomena such as superspreading [1, 16, 21].

We sought to minimize the influence of study-level differences by using individuals from studies with similar experimental procedures (similar species, PCR procedures, etc.), and by developing a Bayesian hierarchical model to capture any systematic differences among studies, but we cannot rule out the possibility that some unwanted strain/species/lab differences contributed to the patterns in our results. There is some evidence from previous studies that cynomolgus macaques experience more severe infections than rhesus macaques following SARS-CoV-1 inoculation [17, 23], but small sample sizes and differences in viral strains in those studies prevented any definitive conclusions. In our case, fitting the dose-response and viral kinetics model to only cynomolgus macaque data resulted in similar parameter estimates except with wider credible intervals compared to when data from both cynomolgus and rhesus macaques were used. For the different SARS-CoV-1 virus strains, it was difficult for us to assess whether there were any strain effects since the only studies that used different strains also used different macaque species. The inferred posterior distributions for

growth and decay rates across the studies and strains in our analysis were all relatively similar (results not reported here), which suggested that the virus strain differences were minor. However, due to limitations in the available data, there was the possibility that our model was unable to distinguish the finer differences in kinetics between the various SARS-CoV-1 strains.

Overall, our study proposes a new approach to studying dose-response relationships and viral kinetics even when data are sparse, and presents the first dose-response analysis of SARS-CoV-1 in NHPs. Despite some limitations in the available NHP SARS-CoV-1 data, we were able to produce useful bounds on the ID_{50} in NHPs and to identify an effect of dose on initial viral load. The joint dose-response and viral kinetics modeling framework we developed is extremely flexible and could be expanded in various ways. In the current model, we have only used viral load data from URT swabs to inform the likelihood, but it would be easy to incorporate additional sources and types of data to compute the probabilities of infection. The hierarchical aspect of our modeling approach allowed us to reuse virological data from multiple previous challenge studies and draw additional insight from the valuable quantitative measurements collected in those experiments. The approach can also be applied to single studies that measure outcomes from multiple dose levels to make better use of the rich data they collect and achieve greater statistical power than standard analyses that treat infection as a binary outcome. This may be particularly valuable in instances where it is unclear how to classify individuals as infected or non-infected. Our modeling framework can be adapted readily to other host-pathogen systems and contributes to a growing movement toward mechanistic analysis of dose-response relationships [7, 8], with the aim of maximizing the scientific value derived from animal experiments and hence reducing the demand for further experiments in line with 3Rs principles [9].

REFERENCES

[1] Pablo M. Beldomenico. "Do superspreaders generate new superspreaders? A hypothesis to explain the propagation pattern of COVID-19". en. In: *International Journal of Infectious Diseases* 96 (July 2020), pp. 461–463. ISSN: 1201-9712. DOI: 10.1016/j.ijid.2020.05.025. URL: https://www.sciencedirect.com/science/article/pii/S1201971220303325 (visited on 05/02/2023).

[2] Jessica A. Belser, Paul A. Rota, and Terrence M. Tumpey. "Ocular Tropism of Respiratory Viruses". In: *Microbiology and Molecular Biology Reviews* 77.1 (Mar. 2013). Publisher: American Society for Microbiology, pp. 144–156. DOI: 10.1128/mmbr.00058-12. URL: https://journals.asm.org/doi/10.1128/MMBR.00058-12 (visited on 06/07/2023).

[3] Michael G Buhnerkempe, Katelyn Gostic, Miran Park, Prianna Ahsan, Jessica A Belser, and James O Lloyd-Smith. "Mapping influenza transmission in the ferret model to transmission in humans". In: *eLife* 4 (Sept. 2015). Ed. by Mark Jit. Publisher: eLife Sciences Publications, Ltd, e07969. ISSN: 2050-084X. DOI: 10.7554/eLife.07969. URL: https://doi.org/10.7554/eLife.07969 (visited on 06/09/2023).

[4] John Carter and Venetia Saunders. "Infectivity Assays". In: *Virology: Principles and Applications*. Wiley, Aug. 2007, p. 23. ISBN: 978-0-470-02386-0.

[5] Yunxin Chen, Li Liu, Qiang Wei, Hua Zhu, Hong Jiang, Xinming Tu, Chuan Qin, and Zhiwei Chen. "Rhesus angiotensin converting enzyme 2 supports entry of severe acute respiratory syndrome coronavirus in Chinese macaques". en. In: *Virology* 381.1 (Nov. 2008), pp. 89–97. ISSN: 0042-6822. DOI: 10.1016/j.virol.2008.08.016. URL: https://www.sciencedirect.com/science/article/pii/S0042682208005230 (visited on 10/28/2021).

[6] Marta L. DeDiego, Lecia Pewe, Enrique Alvarez, Maria Teresa Rejas, Stanley Perlman, and Luis Enjuanes. "Pathogenicity of severe acute respiratory coronavirus deletion mutants in hACE-2 transgenic mice". en. In: *Virology* 376.2 (July 2008), pp. 379–389. ISSN: 0042-6822. DOI: 10.1016/j.virol.2008.03.005. URL: https://www.sciencedirect.com/science/article/pii/S004268220800175X (visited on 06/01/2023).

[7] Katelyn M. Gostic, Elsio A. Wunder, Vimla Bisht, Camila Hamond, Timothy R. Julian, Albert I. Ko, and James O. Lloyd-Smith. "Mechanistic dose–response modelling of animal challenge data shows that intact skin is a crucial barrier to leptospiral infection". In: *Philosophical Transactions of the Royal Society B: Biological Sciences* 374.1782 (Aug. 2019). Publisher: Royal Society, p. 20190367. DOI: 10.1098/rstb.2019.0367. URL: https://royalsocietypublishing.org/doi/full/10.1098/rstb.2019.0367 (visited on 06/09/2023).

[8] Charles N. Haas. "Microbial Dose Response Modeling: Past, Present, and Future". In: *Environmental Science & Technology* 49.3 (Feb. 2015). Publisher: American Chemical Society, pp. 1245–1259. ISSN: 0013-936X. DOI: 10.1021/es504422q. URL: https://doi.org/10.1021/es504422q (visited on 05/04/2023).

[9] Robert C. Hubrecht and Elizabeth Carter. "The 3Rs and Humane Experimental Technique: Implementing Change". en. In: *Animals* 9.10 (Oct. 2019). Number: 10 Publisher: Multidisciplinary Digital Publishing Institute, p. 754. ISSN: 2076-2615. DOI: 10.3390/ani9100754. URL: https://www.mdpi.com/2076-2615/9/10/754 (visited on 06/09/2023).

[10] Sedighe Karimzadeh, Raj Bhopal, and Huy Nguyen Tien. "Review of infective dose, routes of transmission and outcome of COVID-19 caused by the SARS-COV-2: comparison with other respiratory viruses". en. In: *Epidemiology & Infection* 149 (2021). Publisher: Cambridge University Press, e96. ISSN: 0950-2688, 1469-4409. DOI: 10.1017/S0950268821000790. URL: https://www.cambridge.org/core/journals/

epidemiology-and-infection/article/review-of-infective-dose-routes-of-transmission-and-outcome-of-covid19-caused-by-the-sarscov2-comparison-with-other-respiratory-viruses/8607769D2983FE35F15CCC328AB8289D (visited on 05/04/2023).

[11] Matthew Kay. *tidybayes: Tidy Data and Geoms for Bayesian Models*. R package version 3.0.4. 2023. DOI: 10.5281/zenodo.1308151. URL: http://mjskay.github.io/tidybayes/.

[12] James V. Lawler, Timothy P. Endy, Lisa E. Hensley, Aura Garrison, Elizabeth A. Fritz, May Lesar, Ralph S. Baric, David A. Kulesh, David A. Norwood, Leonard P. Wasieloski, Melanie P. Ulrich, Tom R. Slezak, Elizabeth Vitalis, John W. Huggins, Peter B. Jahrling, and Jason Paragas. "Cynomolgus Macaque as an Animal Model for Severe Acute Respiratory Syndrome". en. In: *PLOS Medicine* 3.5 (Apr. 2006). Publisher: Public Library of Science, e149. ISSN: 1549-1676. DOI: 10.1371/journal.pmed.0030149. URL: https://journals.plos.org/plosmedicine/article?id=10.1371/journal.pmed.0030149 (visited on 09/26/2021).

[13] Bao-jian Li, Qingquan Tang, Du Cheng, Chuan Qin, Frank Y. Xie, Qiang Wei, Jun Xu, Yijia Liu, Bo-jian Zheng, Martin C. Woodle, Nanshan Zhong, and Patrick Y. Lu. "Using siRNA in prophylactic and therapeutic regimens against SARS coronavirus in Rhesus macaque". en. In: *Nature Medicine* 11.9 (Sept. 2005). Number: 9 Publisher: Nature Publishing Group, pp. 944–951. ISSN: 1546-170X. DOI: 10.1038/nm1280. URL: https://www.nature.com/articles/nm1280 (visited on 01/04/2021).

[14] L. Liu, Q. Wei, K. Nishiura, J. Peng, H. Wang, C. Midkiff, X. Alvarez, C. Qin, A. Lackner, and Z. Chen. "Spatiotemporal interplay of severe acute respiratory syndrome coronavirus and respiratory mucosal cells drives viral dissemination in rhesus macaques". en. In: *Mucosal Immunology* 9.4 (July 2016), pp. 1089–1101. ISSN: 1935-3456. DOI: 10.1038/mi.2015.127. URL: https://www.nature.com/articles/mi2015127 (visited on 10/28/2021).

[15] Li Liu, Qiang Wei, Qingqing Lin, Jun Fang, Haibo Wang, Hauyee Kwok, Hangying Tang, Kenji Nishiura, Jie Peng, Zhiwu Tan, Tongjin Wu, Ka-Wai Cheung, Kwok-Hung Chan, Xavier Alvarez, Chuan Qin, Andrew Lackner, Stanley Perlman, Kwok-Yung Yuen, and Zhiwei Chen. "Anti–spike IgG causes severe acute lung injury by skewing macrophage responses during acute SARS-CoV infection". en. In: *JCI Insight* 4.4 (Feb. 2019). Publisher: American Society for Clinical Investigation. ISSN: 0021-9738. DOI: 10.1172/jci.insight.123158. URL: https://insight.jci.org/articles/view/123158 (visited on 09/26/2021).

[16] J. O. Lloyd-Smith, S. J. Schreiber, P. E. Kopp, and W. M. Getz. "Superspreading and the effect of individual variation on disease emergence". en. In: *Nature* 438.7066 (Nov. 2005). Number: 7066 Publisher: Nature Publishing Group, pp. 355–359. ISSN: 1476-4687. DOI: 10.1038/nature04153. URL: https://www.nature.com/articles/nature04153 (visited on 05/03/2023).

[17] Josephine McAuliffe, Leatrice Vogel, Anjeanette Roberts, Gary Fahle, Steven Fischer, Wun-Ju Shieh, Emily Butler, Sherif Zaki, Marisa St. Claire, Brian Murphy, and Kanta Subbarao. "Replication of SARS coronavirus administered into the respiratory tract of African Green, rhesus and cynomolgus monkeys". en. In: *Virology* 330.1 (Dec. 2004), pp. 8–15. ISSN: 0042-6822. DOI: 10.1016/j.virol.2004.09.030. URL: https://www.sciencedirect.com/science/article/pii/S0042682204006087 (visited on 10/28/2021).

[18] Paul B. McCray, Lecia Pewe, Christine Wohlford-Lenane, Melissa Hickey, Lori Manzel, Lei Shi, Jason Netland, Hong Peng Jia, Carmen Halabi, Curt D. Sigmund, David K. Meyerholz, Patricia Kirby, Dwight C. Look, and Stanley Perlman. "Lethal Infection of K18-hACE2 Mice Infected with Severe Acute Respiratory Syndrome Coronavirus". In: *Journal of Virology* 81.2 (Jan. 2007). Publisher: American Society for Microbiology, pp. 813–821. DOI: 10.1128/jvi.02012-06. URL: https://journals.asm.org/doi/10.1128/JVI.02012-06 (visited on 06/01/2023).

[19] Noriyo Nagata, Naoko Iwata, Hideki Hasegawa, Yuko Sato, Shigeru Morikawa, Masayuki Saijo, Shigeyuki Itamura, Takehiko Saito, Yasushi Ami, Takato Odagiri, Masato Tashiro, and Tetsutaro Sata. "Pathology and virus dispersion in cynomolgus monkeys experimentally infected with severe acute respiratory syndrome coronavirus via different inoculation routes". en. In: *International Journal of Experimental Pathology* 88.6 (2007), pp. 403–414. ISSN: 1365-2613. DOI: https://doi.org/10.1111/j.1365-2613.2007.00567.x. URL: https://onlinelibrary.wiley.com/doi/abs/10.1111/j.1365-2613.2007.00567.x (visited on 03/30/2021).

[20] T. Poisot. "The digitize package: extracting numerical data from scatterplots". In: *The R Journal* 3.1 (2011), pp. 25–26. URL: http://rjournal.github.io/archive/2011-1/RJournal_2011-1.pdf#page=25.

[21] Julia R. Port, Dylan H. Morris, Jade C. Riopelle, Claude Kwe Yinda, Victoria A. Avanzato, Myndi G. Holbrook, Trenton Bushmaker, Jonathan E. Schulz, Taylor A. Saturday, Kent Barbian, Colin A. Russell, Rose Perry-Gottschalk, Carl I. Shaia, Craig Martens, James O. Lloyd-Smith, Robert J. Fischer, and Vincent J. Munster. *Host and viral determinants of airborne transmission of SARS-CoV-2 in the Syrian hamster*. en. Pages: 2022.08.15.504010 Section: New Results. Feb. 2023. DOI: 10.1101/2022.08.15.504010. URL: https://www.biorxiv.org/content/10.1101/2022.08.15.504010v2 (visited on 06/09/2023).

[22] Anjeanette Roberts, Damon Deming, Christopher D. Paddock, Aaron Cheng, Boyd Yount, Leatrice Vogel, Brian D. Herman, Tim Sheahan, Mark Heise, Gillian L. Genrich, Sherif R. Zaki, Ralph Baric, and Kanta Subbarao. "A Mouse-Adapted SARS-Coronavirus Causes Disease and Mortality in BALB/c Mice". en. In: *PLOS Pathogens* 3.1 (Jan. 2007). Publisher: Public Library of Science, e5. ISSN: 1553-7374. DOI: 10.1371/journal.ppat.0030005. URL: https://journals.plos.org/plospathogens/article?id=10.1371/journal.ppat.0030005 (visited on 05/04/2023).

[23] Thomas Rowe, Guangping Gao, Robert J. Hogan, Ronald G. Crystal, Thomas G. Voss, Rebecca L. Grant, Peter Bell, Gary P. Kobinger, Nelson A. Wivel, and James M. Wilson. "Macaque Model for Severe Acute Respiratory Syndrome". en. In: *Journal of Virology* 78.20 (Oct. 2004), pp. 11401–11404. ISSN: 0022-538X, 1098-5514. DOI: 10.1128/JVI.78.20.11401-11404.2004. URL: https://jvi.asm.org/content/78/20/11401 (visited on 01/04/2021).

[24] Stan Development Team. *RStan: the R interface to Stan*. R package version 2.21.8. 2023. URL: https://mc-stan.org/.

[25] Toru Watanabe, Timothy A. Bartrand, Mark H. Weir, Tatsuo Omura, and Charles N. Haas. "Development of a Dose-Response Model for SARS Coronavirus". en. In: *Risk Analysis* 30.7 (2010). _eprint: https://onlinelibrary.wiley.com/doi/pdf/10.1111/j.1539-6924.2010.01427.x, pp. 1129–1138. ISSN: 1539-6924. DOI: 10.1111/j.1539-6924.2010.01427.x. URL: https://onlinelibrary.wiley.com/doi/abs/10.1111/j.1539-6924.2010.01427.x (visited on 05/04/2023).

[26] Hadley Wickham. *ggplot2: Elegant Graphics for Data Analysis*. Springer-Verlag New York, 2016. ISBN: 978-3-319-24277-4. URL: https://ggplot2.tidyverse.org.

[27] Hadley Wickham, Romain François, Lionel Henry, Kirill Müller, and Davis Vaughan. *dplyr: A Grammar of Data Manipulation*. https://dplyr.tidyverse.org. 2023.

[28] Saber Yezli and Jonathan A. Otter. "Minimum Infective Dose of the Major Human Respiratory and Enteric Viruses Transmitted Through Food and the Environment". en. In: *Food and Environmental Virology* 3.1 (Mar. 2011), pp. 1–30. ISSN: 1867-0342. DOI: 10.1007/s12560-011-9056-7. URL: https://doi.org/10.1007/s12560-011-9056-7 (visited on 05/04/2023).